Excitation Wavelength-Dependent Charge Stabilization in Highly Interacting Phenothiazine Sulfone-Derived Donor-Acceptor Constructs

Manju Sheokand,[a] Ajyal Z. Alsaleh,[b] Francis D'Souza,[*b] and Rajneesh Misra[*,a]

[a]Department of Chemistry, Indian Institute of Technology, Indore 453552, India.

[b]Department of Chemistry, University of North Texas, Denton, TX 76203-5017, USA

E-mail: rajneeshmisra@iiti.ac.in, Francis.Dsouza@unt.edu

Abstract

Prolonging the lifetime of charge-separated states (CSS) is of paramount importance in artificial photosynthetic donor-acceptor (DA) constructs to build the next generation of light energy harvesting devices. This becomes especially important when the DA constructs are closely spaced and highly interacting. In the present study, we demonstrate extending the lifetime of the CSS in highly interacting DA constructs by making use of the triplet excited state of the electron donor and with the help of excitation wavelength selectivity. To demonstrate this, π-conjugated phenothiazine sulfone-based push-pull systems, **PTS2**–**PTS6** have been newly designed and synthesized *via* the Pd-catalysed Sonogashira cross-coupling followed by [2 + 2] cycloaddition-retroelectrocyclization reactions. Modulation of the spectral and photophysical properties of the phenothiazine sulfones ($PTZSO_2$) and terminal phenothiazines (PTZ) was possible by incorporating powerful electron acceptors, 1,1,4,4-tetracyanobutadiene (TCBD) and cyclohexa-2,5-diene-1,4-diylidene-expanded TCBD (exTCBD). The quadrupolar **PTS2** displayed solvatochromism, aggregation-induced emission, and mechanochromic behaviors. From the energy calculations, excitation wavelength-dependent charge stabilization was envisioned in **PTS2**–**PTS6** and the subsequent pump-probe spectroscopic studies revealed charge stabilization when the systems were excited at the locally excited (LE) peak positions while such effect was minimal when the samples were excited at wavelengths corresponding to the CT transitions. This work reveals the impact of wavelength selectivity to induce charge separation from the triplet excited state in ultimately prolonging the lifetime of CCS in highly interacting push-pull systems.

Introduction

Following the early events occurring in natural photosynthesis,[1] the study of artificial photosynthetic multi-modular DA constructs[2-9] has played a prominent role in the production of π-conjugated systems useful for a range of applications in energy harvesting, organic electronics, and photonics.[9-18] In this context, close proximity and high exergonicity of DA constructs can be utilized to facilitate intramolecular charge transfer (ICT) and fine-tuning of the optical and excited-state properties,[19-20] however, excited state CS and charge recombination (CR) processes in such systems occur rapidly, making them less appealing in light energy harvesting applications. In synthetic artificial photosynthetic systems, long-lived CSS is often achieved by optimal positioning of the donor and acceptor systems and by following a multi-step sequential electron transfer mechanism.[21-26] In a few instances, heavy atom-bearing triplet sensitizers have also been used,[27-28] however, such strategy in the directly connected highly interacting DA constructs has been nonexistent.

The TCBD and exTCBD-based directly connected DA push-pull systems[29-30] show strong ICT covering absorption in the visible and near IR regions, that is, exhibiting optical properties of black absorbers. Photosensitizers such as porphyrins, phthalocyanines, subphthalocyanines, BODIPYs, azaBODIPYs, triphenylamine, phenothiazine, and diketopyrrolopyrroles have been used in these constructions to extend the optical coverage into the visible and near-IR region.[31-49] Sadly, owing to close proximity and high exergonicity, the excited state CS and CR in these systems occurred within a few picoseconds.[31-50] Extending the lifetime of the CSS in these systems thus far has been a challenge. In the present study, we have overcome this issue, by designing multi-modular DA systems derived from a bis-phenothiazine-phenothiazine sulfone (PTZ-PTZSO_2-PTZ, **PTS2** in Figure 1) scaffold. Introducing TCBD and exTCBD into **PTS2** (**PTS3**–**PTS6** in Figure 1) modulates the energy levels of the DA constructs in such a way that the charge transfer process can be initiated from the ^{3}PTZ* state[50] when they are excited at wavelengths corresponding to the locally excited (LE) states. Owing to the spin-forbidden CR process, long-lived CSSs are observed. Interestingly, when the molecules are excited at the ICT peak positions, the CSS of the singlet character revealed ultrafast CR (spin allowed process) without prolonging its lifetime. This study has provided us with an opportunity to modulate the kinetics of electron

transfer to secure the much-desired long-lived CSSs as a function of excitation wavelength in highly interacting DA constructs.

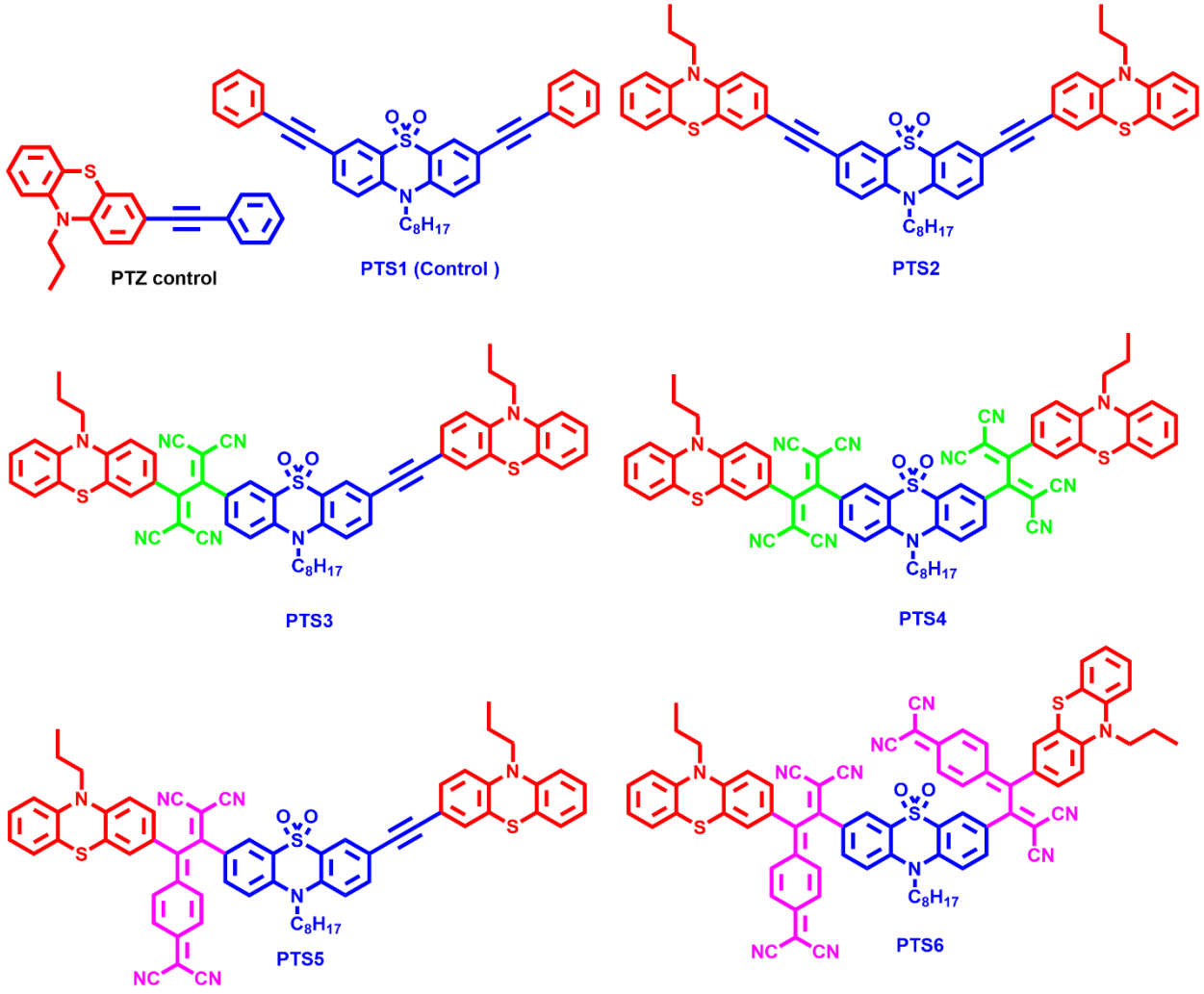

Figure 1. The molecular structures of phenothiazine sulfone-based push-pull constructs.

Experimental section

General methods

All the chemicals were used as received unless otherwise indicated. The oxygen or moisture-sensitive reactions were performed under a nitrogen/argon atmosphere using the standard schlenk method. All the chemicals were purchased from commercial sources and used without further purification. ^{1}H NMR (400 MHz), and ^{13}C NMR (100MHz) spectra were recorded on the Bruker Avance (III) 400 MHz, using $CDCl_3$ as the solvent and the chemical shifts were reported

in parts per million (ppm). Tetramethylsilane (TMS) was used as an internal reference for recording ^{1}H (of the residual proton; δ = 7.26 ppm), and ^{13}C (δ = 77.0 ppm) spectra in $CDCl_3$. At IIT-I, UV-visible absorption spectra of all compounds in Dichloromethane were recorded on a Carry-100 Bio UV-visible Spectrophotometer. HRMS was recorded on Brucker-Daltonics, micrO TOF-Q II mass spectrometer.

The UV-visible spectral measurements were carried out with a Shimadzu Model 2550 double monochromator UV-visible spectrophotometer. The fluorescence and phosphorescence spectra were recorded using a Horiba Yvon Nanolog coupled with time-correlated single-photon counting with nanoLED excitation sources. A right-angle detection method was used. Differential pulse and cyclic voltammograms were recorded on an EG&G 263A electrochemical analyzer using three-electrode system. A platinum button electrode was used as the working electrode. A platinum wire served as the counter electrode and an Ag/AgCl electrode was used as the reference electrode. Ferrocene/ferrocenium redox couple was used as an internal standard. All the solutions were purged prior to electrochemical and spectral measurements using argon gas.

Femtosecond transient absorption spectroscopy experiments were performed using an ultrafast femtosecond laser source (Libra) by Coherent incorporating a diode-pumped, modelocked Ti:sapphire laser (Vitesse) and a diode-pumped intracavity doubled Nd:YLF laser (Evolution) to generate a compressed laser output of 1.45 W. For optical detection, a Helios transient absorption spectrometer coupled with a femtosecond harmonics generator, both provided by Ultrafast Systems LLC, was used. The sources for the pump and probe pulses were derived from the fundamental output of Libra (Compressed output 1.45 W, pulse width 100 fs) at a repetition rate of 1 kHz; 95% of the fundamental output of the laser was introduced into a TOPAS-Prime-OPA system with a 290−2600 nm tuning range from Altos Photonics Inc., (Bozeman, MT), while the rest of the output was used for generation of a white light continuum. Kinetic traces at appropriate wavelengths were assembled from the time-resolved spectral data. Data analysis was performed using Surface Xplorer software supplied by Ultrafast Systems. All measurements were conducted in degassed solutions at 298 K. The estimated error in the reported rate constants is ±10%.

Results and Discussion

Synthesis highlights

PTS2 bearing two terminal PTZ units and a central $PTZSO_2$ was synthesized as the starting material for introducing TCBD and exTCBD entities. The synthesis of **PTS2** was carried out *via* the Pd-catalyzed Sonogashira cross-coupling reaction of dibromo-substituted phenothiazine sulfone **1** with 2.2 equivalent of ethynyl phenothiazine **2** in THF/TEA (1:1) solvent at 70 ºC for 12 h. Following purification by column chromatography, **PTS2** was obtained with 76% yield (Scheme 1). The starting compounds, bromo-substituted $PTZSO_2$, **1** and ethynyl phenothiazine, **2** were synthesized using reported procedures.[51] A control compound, **PTZ-control**, with phenyl rings as the end-capping unit has also been synthesized.

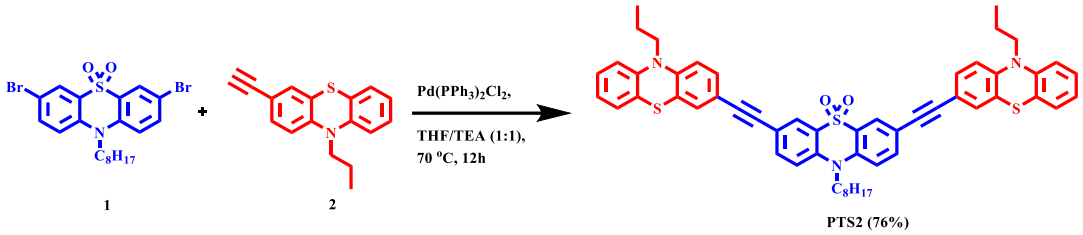

Scheme 1. Synthetic route of symmetrical phenothiazine sulfone based chromophores **PTS2**.

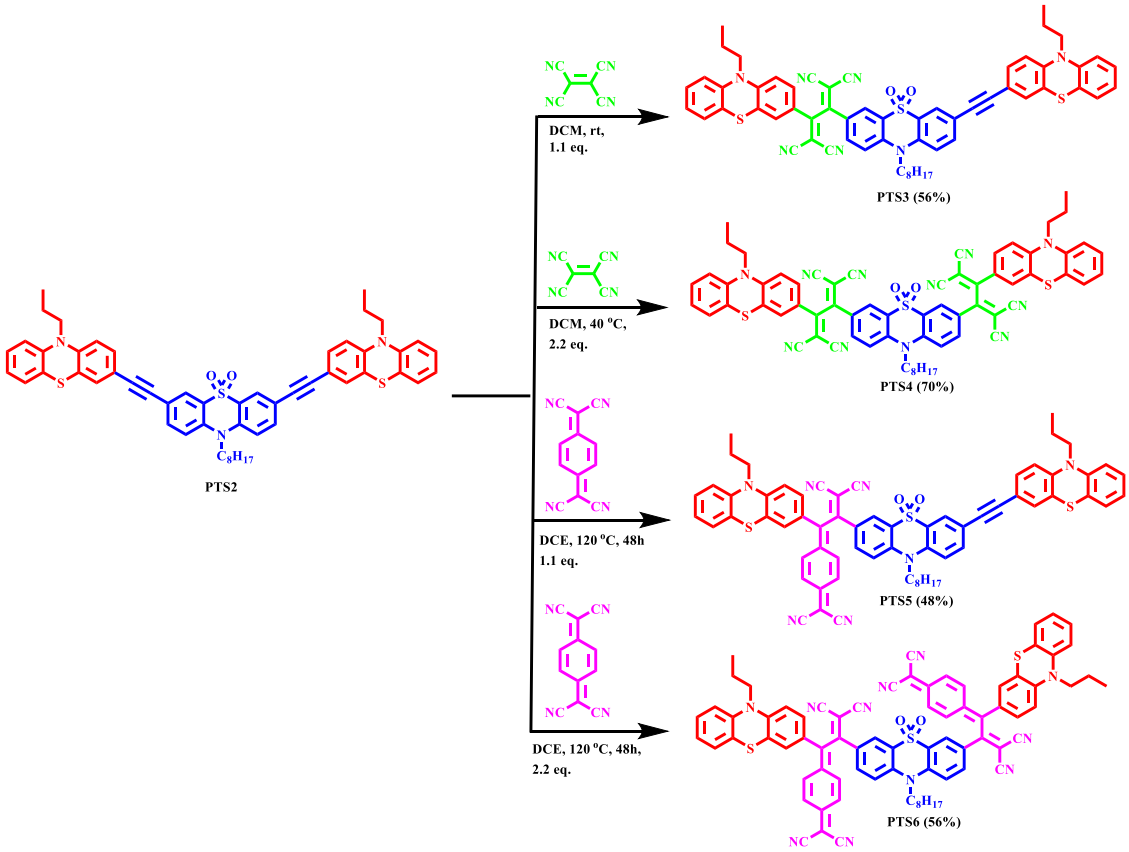

Scheme 2. Synthetic route of symmetrical and unsymmetrical PTZSO$_2$-based push-pull **PTS3**–**PTS6**.

The TCBD and exTCBD featured phenothiazine sulfone DA constructs, **PTS3**–**PTS6**, were synthesized *via* the Pd-catalyzed Sonogashira cross-coupling reaction and [2+2] cycloaddition−retroelectrocyclization reaction. Here, we have varied the acceptor from mono-TCBD to bis-TCBD in **PTS3–PTS4**, and additionally exploited the exTCBD unit from mono-exTCBD to bis-exTCBD in **PTS5–PTS6**. The [2 + 2] cycloaddition−retroelectrocyclization reaction[29-30] of chromophore **PTS2** with 1.1 equivalent of TCNE in dichloromethane solvent for 24 h at room temperature resulted in unsymmetrical chromophore **PTS3** in 56% yield, whereas the reaction of **PTS2** with 2.2 equivalent of TCNE resulted in symmetrical chromophore **PTS4** in 70% yield. The expanded TCBD functionalized unsymmetrical chromophore **PTS5** was synthesized *via* [2 + 2] cycloaddition−retroelectrocyclization reaction of **PTS2** with 1.1 equivalent of TCNQ in DCE solvent for 48 h at 120 ºC in 48% yield. The reaction of **PTS2** with 2.2 equivalent of TCNQ resulted in the expanded TCBD functionalized symmetrical chromophore **PTS6** in 56% yield (Scheme 4). The synthetic procedure for control compound **PTS1** is given in Scheme S1 (SI). The characterization of all the newly synthesized compounds was carried out using ^{1}H and ^{13}C NMR spectroscopy and the HRMS technique (see Figures S11 – S31 in SI)

Absorption Spectra

The optical properties of the **PTS1**–**PTS6** constructs were recorded in dichloromethane as shown in Figure 2 and the data are listed in Table 1. The absorption spectrum of symmetrical **PTS2** shows an absorption band at 389 nm, which is attributed to the π–π* transition. The absorption spectra of TCBD functionalized unsymmetrical and symmetrical chromophores, **PTS3** and **PTS4** exhibited multiple absorption bands (300−460 nm) in the lower wavelength region attributed to the π–π* electronic transitions. The broad absorption band for **PTS3** and **PTS4** at the longer wavelength of 570 nm and 546 nm, respectively, is ascribed to the ICT transitions (also known as intramolecular charge polarization) due to the strong D-A push-pull interactions. The symmetrical chromophore **PTS4** showed a comparatively broad ICT band compared to the unsymmetrical

Table 1: Photophysical and electrochemical data of chromophores **PTS1**–**PTS6** recorded in dichloromethane solution.

Compound	$\lambda_{abs,}$ nm $\varepsilon/10^5(M^{-1}cm^{-1})$	HOMO (eV)[a]	LUMO (eV)[a]	ΔE^a	ΔE_g (HOMO–LUMO gap)[b]
PTS2	381 (54140)	−5.06	−2.60	1.81	3.40
PTS3	456 (26140), 570 (10160)	−5.34	−4.15	1.04	2.09
PTS4	450 (38390), 546 (18410)	−5.59	−4.25	1.21	2.05
PTS5	406 (35410), 660 (14240)	−5.31	−4.21	0.98	1.46
PTS6	448 (15570), 663 (7850)	−5.42	−4.23	0.96	1.62

[a] HOMO-LUMO energy gap from electrochemical studies by using the cyclic voltammetry

[b] theoretical energy gap calculated from density functional theory.

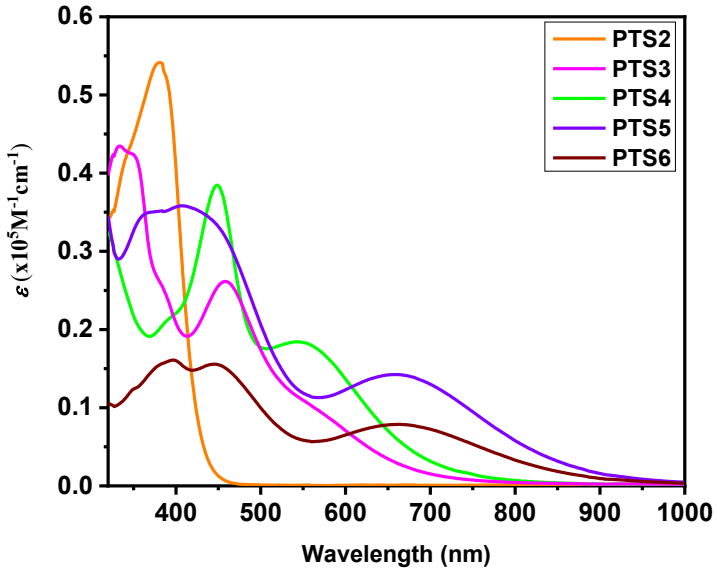

Figure 2. Electronic absorption spectra of **PTS2**–**PTS6** donor-acceptor constructs in dichloromethane.

PTS3 owing to the incorporation of an additional TCBD unit. The chromophores **PTS5** and **PTS6** incorporated with exTCBD acceptor showed a broad absorption in the longer wavelength region

of 550−1000 nm which could be attributed to the ICT transitions and the absorption band around 400 nm in the lower wavelength region to the π–π* electronic transitions. The ICT band of **PTS5** and **PTS6** was red-shifted by 90–120 nm due to the incorporation of stronger acceptor exTCBD units than the chromophores **PTS3** and **PTS4** having comparatively weaker TCBD (*vide supra*).

Solvatochromism

The effect of solvents of different polarities on the ICT transition of **PTS2** was investigated through absorption and emission spectroscopy (Figure 3). The ICT transition is expected to enhance the dipole moment of the molecule in the excited state resulting in a polarized excited state.[19-20] The reorganization of polar solvent molecules around the polarized excited state results in the stabilization of the excited state which is observed *via* the redshift in the emission spectrum of **PTS2** on varying the solvent polarity from non-polar (cyclohexane, toluene) to polar solvent (1,4-dioxane, THF, chloroform, dichloromethane (DCM)). In contrast to the absorption spectra (see Figure S1), the emission spectra of **PTS2** exhibit noticeable change due to the formation of a more polarized excited state than the electronic ground states. In the non-polar solvent, *i.e.* cyclohexane, a blue color emission was recorded at 453 nm with a shoulder peak at

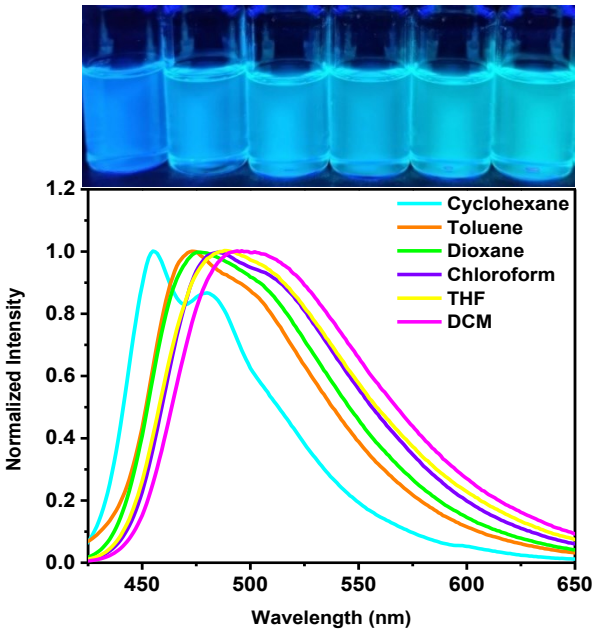

Figure 3. The normalized emission spectrum of **PTS2** in solvents of varying polarities.

479 nm owing to the localized excited (LE) emission. On increasing the solvent polarity from toluene to DCM, the peak corresponding to LE emission was merged into CT emission, and a broad spectrum with emission maxima was recorded at 473 nm (toluene), 475 nm (1,4-dioxane), 483 nm (chloroform), 488 nm (THF), and 497 nm (DCM), respectively. The chromophores **PTS3**–**PTS6** were non-emissive in the solvents of varying polarities as emission gets quenched by the incorporation of TCBD and exTCBD electron acceptor units.

Aggregation-Induced Emission (AIE)

The **PTS2** exhibits aggregation-induced emission owing to the AIE active butterfly-shaped phenothiazine unit, which shows strong yellow color emission in the solid-state.[52] The **PTS2** is readily soluble in DMF and the gradual increase of water fraction in DMF results in the formation of nano-aggregates. The **PTS2** exhibits a light yellow color emission at 524 nm in pure DMF. The addition of water up to 30% results in a gradual decrease in the intensity of emission spectra which is likely due to additional solvent stabilization of the CT state. At a 40% water fraction, a new emission peak appeared at 563 nm, which showed a redshift of 39 nm. The enhanced emission at

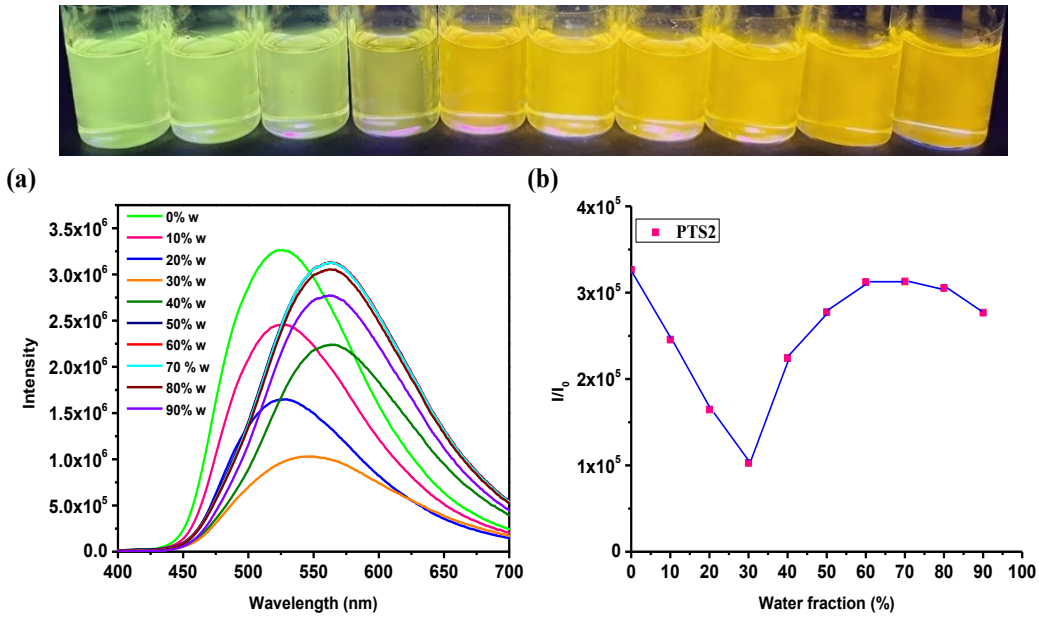

Figure 4. (a) Emission spectrum of **PTS2** in DMF–water mixtures (0–90% water), and (b) plot of fluorescence intensity *vs.* % of water fraction (f_w) (**PTS2** concentration = 10 μM; intensity was calculated at λ_{max}). The top panel shows a picture of the **PTS2** solution in DMF on increasing the addition of water under UV-light illumination.

40% water fraction could be assigned to the formation of nano-aggregates, and the intensity of AIE gradually increases up to 70% water fraction. At high water concentrations, a slight decrease in the emission intensity was observed, which is attributed to the formation of large-sized nano-aggregates, which are less exposed to radiation as compared to smaller aggregates. The AIE behavior was also studied using absorption spectroscopy (Figure S2, SI). The absorption spectra for chromophore **PTS2** revealed no significant change up to 60% water fraction, above which there was a scattering of light or the Mie effect[57] (also known as non-molecular scattering or aerosol particle scattering) observed due to the formation of nanoaggregates. The AIE behavior of **PTS2** is shown in Figure 4 under UV illumination. The chromophores **PTS3–PTS6** incorporated with TCBD and exTCBD units are not fluorescent in the solid-state and were not susceptible to exhibit AIE behavior.

Mechanochromism

Compound **PTS2** was predicted to exhibit mechano-responsive behavior owing to the conformationally flexible butterfly-shaped phenothiazine moiety in the molecular framework.[52-53] The attachment of phenothiazine units *via* triple bond at 3 and 7 positions could enhance the

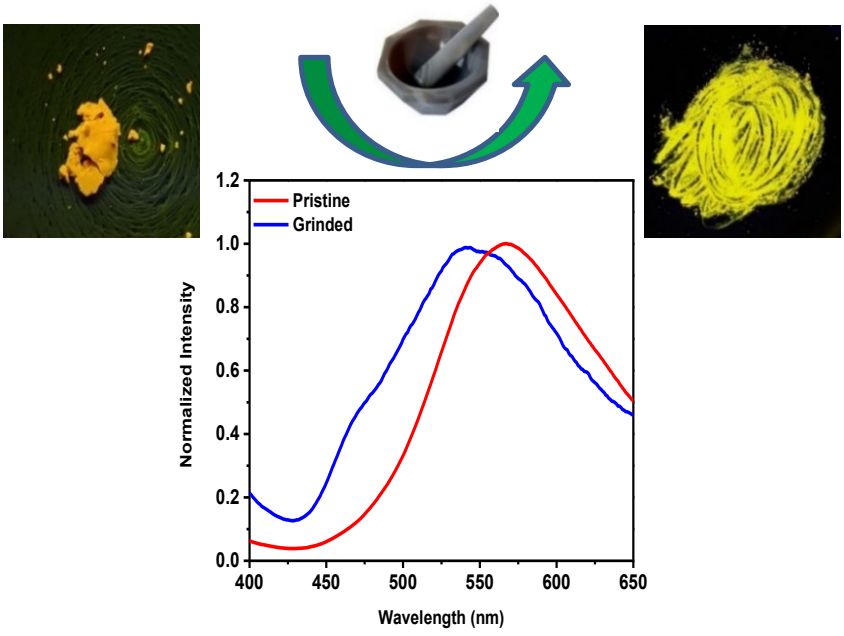

Figure 5. Solid state emission of **PTS2** in the pristine and milled form.

flexibility of donor phenothiazine unit around the central phenothiazine sulfone moiety and promote physical structural change owing to a twisted structure on applying the mechanical stimuli. The pristine form of **PTS2** is light orange in color and emits at 568 nm. The application of mechanical grinding of **PTS2** resulted in bright yellow emission at 540 nm (Figure 5). The powder X-ray diffraction (PXRD) of **PTS2** in the pristine and ground state, shown in Figure S3, revealed the amorphous nature of **PTS2** in both states and there is no major structural change upon grinding the material.

Theoretical Studies

The density functional theory (DFT) calculations on **PTS2–PTS6** were performed to optimize the molecular geometry and electronic properties using the B3LYP/6-31G** basis set.[54] In order to reduce the computation time, the propyl substituent was used instead of the octyl substituent at the central $PTZSO_2$. The TCBD and exTCBD substituted chromophores **PTS3–PTS6** exhibited a non-planar framework owing to the presence of a butterfly-shaped $PTZSO_2$ unit as the central core and additional acceptor TCBD units (Figure 6). The frontier orbitals of **PTS2**–**PTS6** are shown in Figure 6. The HOMO energy level in **PTS2** is distributed throughout the molecule but the LUMO is concentrated mostly on the $PTZSO_2$ unit with some contributions to the terminal phenothiazine entities. In the unsymmetrical chromophores **PTS3** and **PTS5**, the electron density of the HOMO is mainly concentrated on the terminal PTZ unit with some coefficients on the benzene ring of the central $PTZSO_2$. In these molecules, the LUMO is predominantly concentrated on the acceptor TCBD unit and extended toward the central $PTZSO_2$ unit. In the case of TCBD functionalized symmetrical chromophores **PTS4** and **PTS6**, the electron density of the HOMO energy levels was mainly concentrated on the terminal donor PTZ unit. The incorporation of additional TCBD or exTCBD in **PTS4** and **PTS6** tends to increase the acceptor character and the LUMO energy levels were localized on the TCBD unit. The outcomes of the theoretical calculations show excellent intramolecular electronic communication. The electron-withdrawing character of the TCBD/exTCBD acceptor units caused a significant decrease in the HOMO–LUMO energy gap in **PTS2**–**PTS6**. The theoretically calculated HOMO–LUMO gaps for **PTS2–PTS6** are 3.44, 1.94, 2.19, 1.49, and 1.69 eV, respectively. These values are in good agreement with experimental data

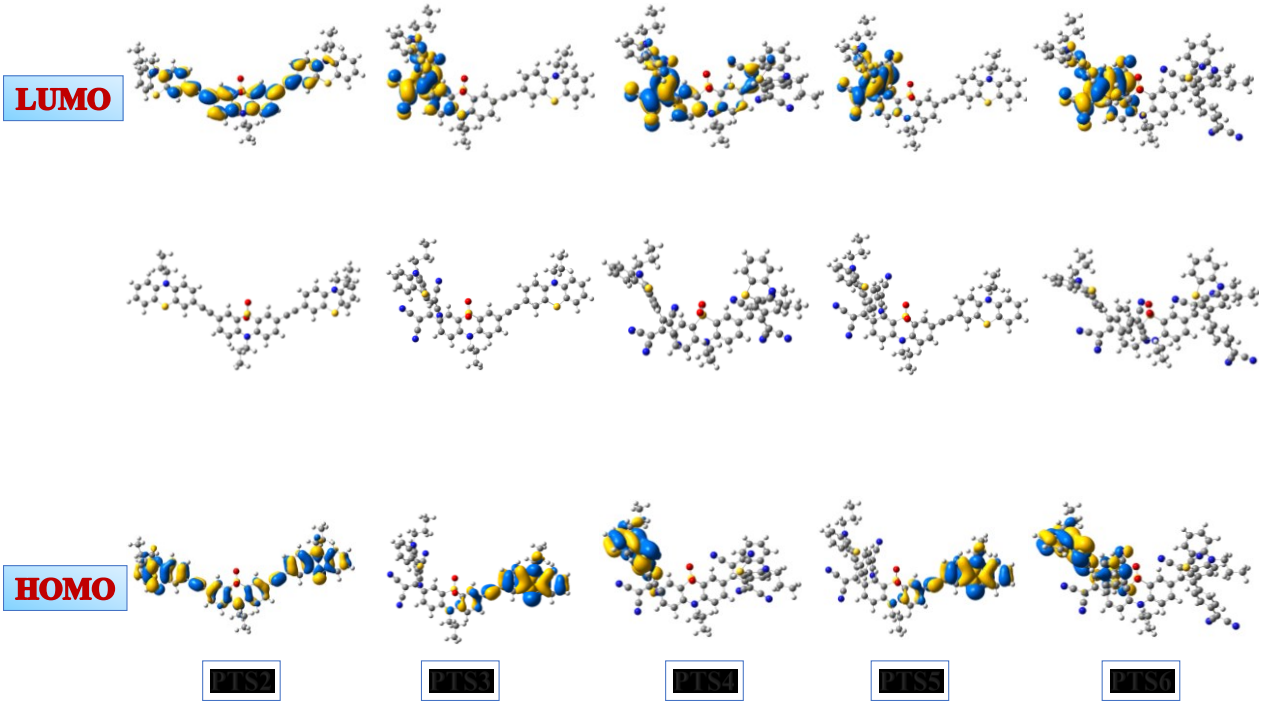

Figure 6. Optimized structure, frontier HOMO and LUMO orbitals of **PTS2**–**PTS6**.

calculated from the electrochemical studies (*vide supra*). The HOMO–LUMO gap in **PTS2**–**PTS6** follows the order **PTS2** > **PTS4** > **PTS3** > **PTS6** > **PTS5**, which is reflected in their electronic absorption. The chromophore **PTS2** with a high HOMO–LUMO gap has exhibited absorption in the lower wavelength region, whereas the TCBD/exTCBD functionalized **PTS3**–**PTS6** showed red-shifted absorption in the NIR region due to the tuned HOMO–LUMO gap.

Electrochemical Studies

The redox properties of chromophores **PTS1**–**PTS6** were evaluated by the means of cyclic voltammetry (CV) in o-dichlorobenzene (DCB) containing 0.1 M $TBA(ClO)_4$ as a supporting electrolyte. The voltammograms are shown in Figure S4 and the peak potentials are listed in Table S1 while the calculated energy gap (difference between the first oxidation and first reduction) is given in Table 1. **PTZ-control** with only a PTZ entity revealed oxidation at 0.81 V vs. Ag/AgCl corresponding to $PTZ^{0/.+}$ process. **PTS1** with only a $PTZSO_2$ group revealed a quasi-reversible reduction at -0.95 V vs. Ag/AgCl suggesting it is fairly electron-deficient due to the sulfone group. Irreversible oxidation at E_{pa} = 1.63 V was also observed. The oxidations of PTZ entities in **PTS2** were located at 0.86 and 1.36 V while the reduction corresponding to the central $PTZSO_2$ was at -

0.95 V. The electron donor role of PTZ and acceptor role of $PTZSO_2$ in **PTS2** is thus born out. In the cases of **PTS3** and **PTS4**, with one and two entities of TCBDs, additional cathodic processes corresponding to TCBD reductions were observed. In **PTS3**, two reductions at -0.16 and -0.54 V corresponding to $TCBD^{0/\cdot-}$ and $TCBD^{\cdot-/2-}$ were witnessed while the PTZ oxidation was slightly anodically shifted and appeared at 0.88 and 1.06 V. The first oxidation was due to the PTZ entity far from TCBD and the second peak was due to PTZ close to TCBD. An anodic shift of about 180 mV in the latter process is due to the electronic effect induced by the neighboring TCBD entity. In the case of **PTS4**, although the TCBD reductions appeared to have almost the same potential, the PTZ oxidation appeared as a single peak at 1.07 V as both PTZ entities were close to TCBD. In the case of **PTS5** and **PTS6**, having one and two entities of exTCBDs, reductions corresponding to the exTCBD occurred at much lower potentials compared to that observed for TCBD in **PTS3** and **PTS4**. The first two reductions of exTCBD in **PTS5** were located at -0.03 and -0.13 V and oxidation at 0.95 V corresponding to PTZ entities (overlap of two anodic waves) were observed. A similar trend was also observed for **PTS6**. In this case, exTCBD reductions were at -0.01 and -0.13 V, and the first oxidation corresponding to phenothiazine was at 0.90 V. The electrochemical redox gap, ΔE, followed the order: **PTS6** < **PTS5** < **PTS3** < **PTS4** < **PTS2**. This trend agrees well with the optical coverage of these compounds displayed in Figure 2.

Energy Consideration for Excited-State Electron Transfer

In benzonitrile (solvent used in photochemical studies, see Figure S32 for absorption and fluorescence spectra), **PTS2**, absorption, and fluorescence peak maxima were located at 370 and 500 nm, respectively, not significantly different from that observed in DCB, from which an $E_{0,0}$ value of 2.90 eV was calculated. The phosphorescence spectrum of **PTS1** is shown in Figure S5. Triplet emission at 520 nm was observed from which energy of the triplet state, E_T = 2.38 eV was obtained. The singlet lifetime of **PTS2**, from the time-correlated single-photon counting (TCSPC) technique, was found to be 4.6 ns which was smaller than that of **PTS1** being 5.8 ns (both monoexponential decays), suggesting the occurrence of excited state events in **PTS2** (see Figure S6 for decay curves). The absorption and emission spectra of **PTZ-control** are shown in Figure S7. Absorption peak maxima at 349 nm, fluorescence peak maxima at 460 nm, and phosphorescence (at liquid nitrogen temperature) at 532 nm was observed. The singlet lifetime of **PTZ-control** from the TCSPC technique revealed a monoexponential decay with a lifetime of

5.09 ns. From the phosphorescence peak maxima, triplet energy for ^{3}PTZ* was calculated to be 2.32 eV. In order to visualize the possibility of excited-state charge transfer, using the optical, computational, and redox data, energy level diagrams were established. Free-energy of charge separation and charge recombination was estimated using the Rehm-Weller approach.[55] Figures 7a and b, respectively show the energy level diagrams of **PTS2**, and TCBD-derived systems (**PTS3** and **PTS4**), while Figure S8 shows exTCBD-derived systems (**PTS5** and **PTS6**).

As shown in Figure 7a, in the case of the quadrupolar **PTS2** system comprised of two PTZ electron donors and one $PTZSO_2$ electron acceptor, photoinduced electron transfer (PET) from both singlet and triplet excited states yielding $PTZ^{\cdot+}$- $PTZSO_2^{\cdot-}$-PTZ charge-separated state in benzonitrile is thermodynamically possible. The relatively high energy of ^{3}PTZ* (2.32 eV) or $^3PTZSO_2$* (2.38 eV) formed from the intersystem crossing of the respective singlet excited states was realized to be an important contributor. If electron transfer indeed originates from the ^{3}PTZ* or $^3PTZSO_2$* then the charge-separated state would also be a triplet state. Under such circumstances, charge recombination would be a slow process as this is a spin-forbidden process. Relatively long-lived charge-separated states could be anticipated from such a process.

The energy diagrams for systems showing strong charge transfer events are shown in Figures 7b and S8. From the earlier discussed optical data, two types of excitation processes, viz., local excitation (LE) and charge transfer (CT), are possible in both TCBD and exTCBD possessing systems. The energy of the CT state evaluated from computational results (energy difference between HOMO and LUMO levels) and CS state from the traditional Rehm-Weller approach (including the energy of solvation from the Dielectric continuum model)[49] are utilized in the construction of these diagrams. It is important to note that both E_{CT} and E_{CS} are well-below those of both E_S and E_T energies under the conditions of LE excitation. Under such circumstances, ^{3}PTZ* formed upon intersystem crossing (ISC) of ^{1}PTZ* can involve in the CT and CS processes resulting in the radical ion-pair formation of triplet character. However, when these systems are excited at longer wavelengths corresponding to CT peak maxima, the E_{CT} would be much lower than either E_{CT} or E_{CS} states. If ET occurs, the resulting CS product will be of singlet character, and under such circumstances, faster CR to the ground state could be expected due to the singlet nature of the product, lowering the overall lifetime of the CSS. Importantly, due to the high exergonicity of the CS events, much faster electron transfer events could also be anticipated. It may be mentioned here that in a recently reported study by us featuring PTZ monomer and dimer

carrying TCBD and exTCBD, the E_T and E_{CT} were almost the same, especially in the case of TCBD systems, creating a ping-pong effect between triplet and charge-transfer states.[49] The present study with a central $PTZSO_2$ seems to lower the E_{CT} energy facilitating CT and CS originating from the triplet state.

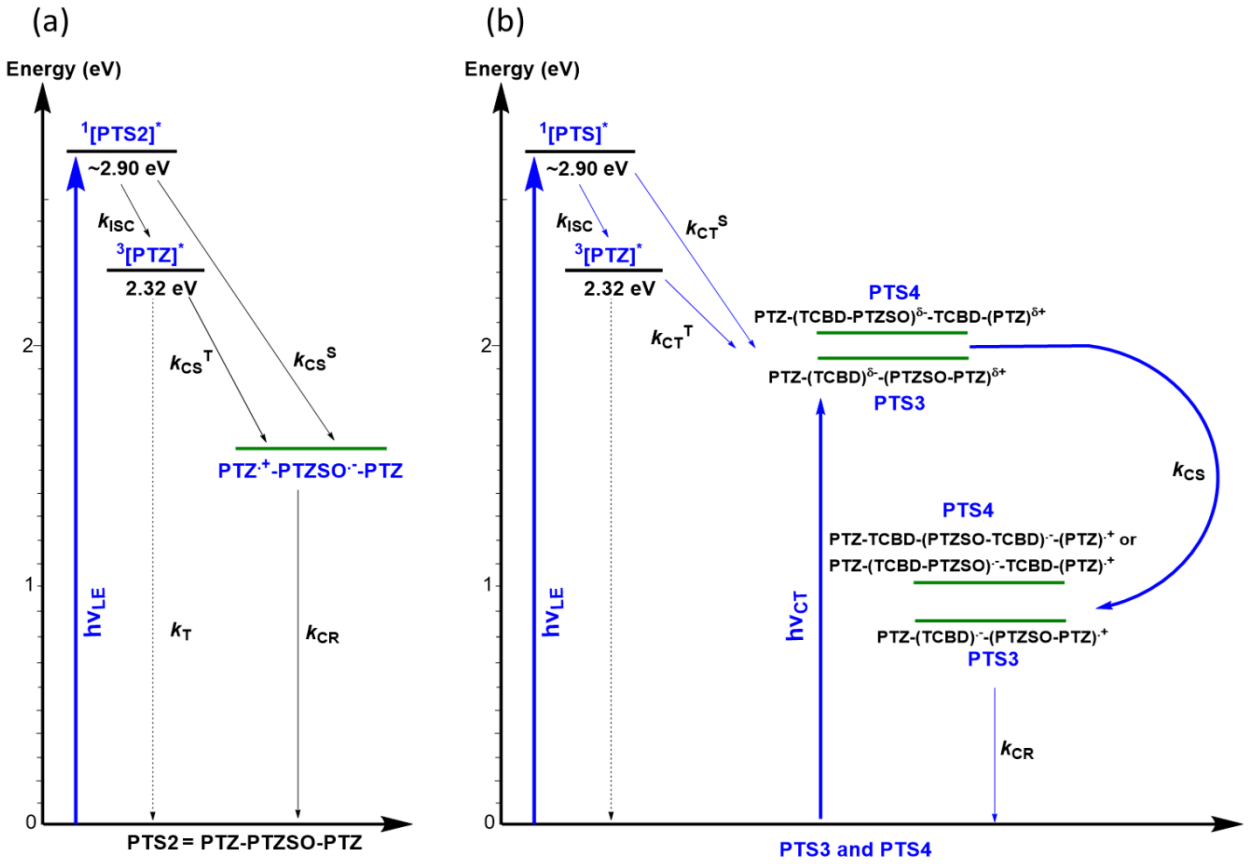

Figure 7. Energy level diagrams showing different photochemical events in (a) **PTS2** triad and (b) TCBD bearing systems under local excitation (LE) and charge transfer (CT) peak positions (see text for details). Note - Excitation of **PTS3** and **PTS4** corresponding to their CT would produce their singlet excited states, not shown for brevity.

Femtosecond Transient Absorption Studies

Pump-probe spectroscopic studies using 100 fs laser pulses of selected wavelengths are subsequently performed to witness the charge transfer/separation and kinetics as a function of excitation wavelengths involving the LE and CT peak positions. In order to help interpret the transient spectral results, the oxidized and reduced species of the investigated compounds were generated as shown in Figure S9. The oxidized species of **PTZ2** exhibited a low-intensity new

peak at 470-550 nm, however, no new peaks were observed during the reduction of **PTZ2**. The oxidized species of **PTS3** and **PTS4** revealed a new peak in the 600 nm region while the reduced species revealed a broad peak spanning the 500–800 nm range. Similarly, a new peak in the 980 nm region for the oxidized species of **PTS5** and **PTS6**, new peaks at 645, and a broad peak spanning 880–1400 nm with peak maxima at 1142 nm for the reduced species were observed.

Figure 8a shows the femtosecond transient absorption (fs-TA) spectra at the indicated delay times for **PTZ-control** in benzonitrile at the excitation wavelength of 395 nm. The ^{1}PTZ* formed was characterized by a broad negative signal covering the 480–500 nm range, and from the earlier discussed spectral data, this has been attributed to the process of stimulated emission (SE). Recovery of this signal was slow consistent with its long singlet lifetime of 5.09 ns. The recovery was associated with the slow growth of a new signal in the 580–600 nm which could be attributed

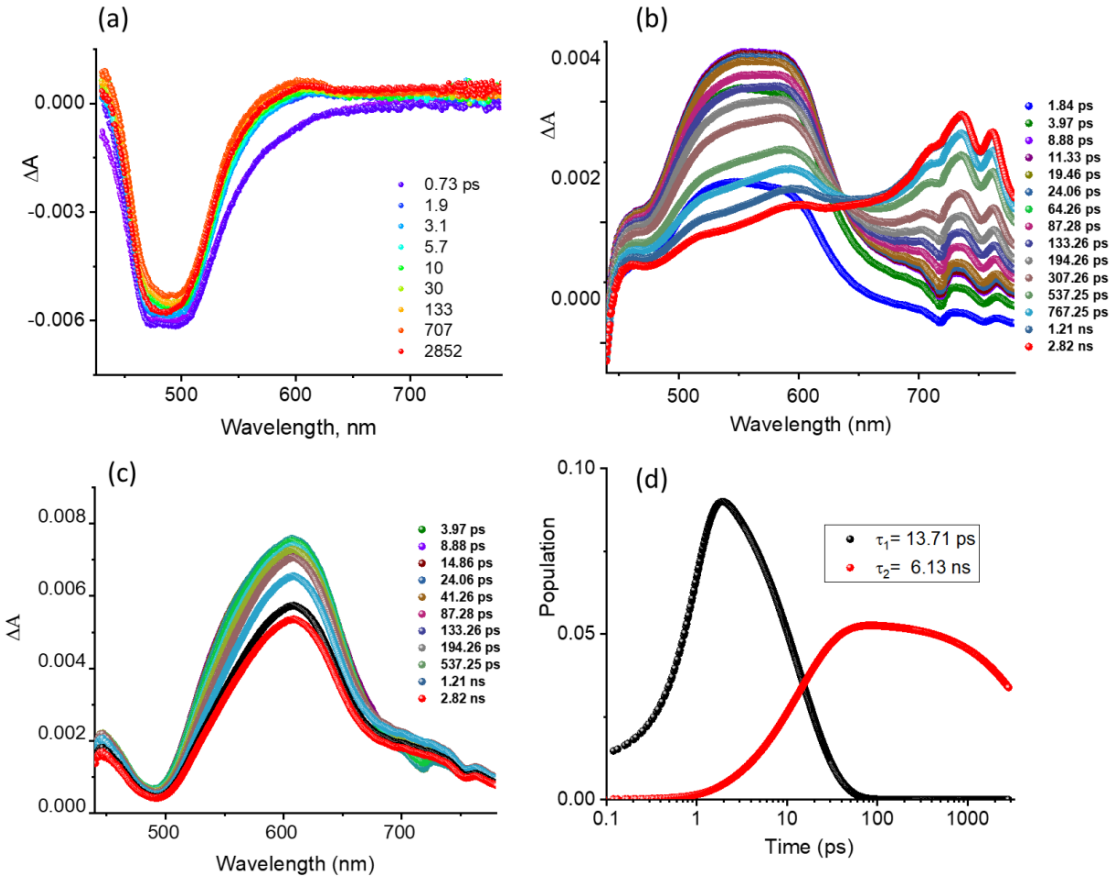

Figure 8. Fs-TA spectra at the indicated delay times of (a) **PTZ-control** (excitation = 395 nm), (b) **PTS1** (excitation = 366 nm) and (c) **PTS2** (excitation = 366 nm) in PhCN. Figure (d) shows the population kinetics of different photo-events of **PTS2**.

to the ^{3}PTZ*. In the case of **PTS1** having only a $PTZSO_2$, the fs-TA spectral features were different (see Figure 8b). A strong excited state absorption peak (ESA) spanning the 500–600 nm region was observed with a negative peak in the 490 nm range due to SE. Decay/recovery of the positive and negative signals was accompanied by new peaks at 520, 600, 734, and 761 nm attributable to the triplet excited state.

The fs-TA spectra of the triad **PTS2** having two PTZ and a central $PTZSO_2$ are shown in Figure 8c. It may be mentioned here that at the excitation wavelength of 366 nm both chromophores are likely to get excited resulting in oxidative (from excited PTZ) and reductive (from excited $PTZSO_2$) electron transfer events. From Figure 7a, charge separation from both the singlet and the triplet excited states was expected although the latter would be the primary contributor. The transient spectra revealed a strong peak at 606 nm with small spectral shifts during the course of the experiment. Since both ^{3}PTZ* and $PTZ^{\cdot+}$ signals are expected in this region, from the spectral trends, the presence of both ^{3}PTZ* and $PTZ^{\cdot+}$ at the earlier delay times and only $PTZ^{\cdot+}$ at the latter time was obvious. That is, ^{3}PTZ* and $^3PTZSO_2$* involvement in CS and not their singlet excited states was obvious. Expectedly, $^3PTZSO_2$* peaks, expected in the 520, 600, 734, and 761 nm range (see Figure 8b), were absent further confirming its involvement in the charge separation process. The majority of the signal persisted beyond the 3 ns, the delay time of our instrument setup, further supporting the CS process to originate from the triplet excited state. The data was further subjected to global target analysis[56-57] wherein both two-component fit (representing $T_1 \rightarrow$ CS) and three-component fit (representing $S_1 \rightarrow T_1 \rightarrow$ CS) was applied. The lifetime of the long- lived component, attributable to the CS state was 6.13 ns, however, this could be considered the lower limit as much of the signal was still present. Next, the push-pull systems derived from TCBD, **PTS3,** and **PTS4**, were investigated by exciting the sample at 400 nm corresponding to the LE state. As shown in Figure 8b, at this excitation wavelength, the ^{1}PTZ* is expected to undergo ISC to produce ^{3}PTZ* that would eventually promote CT and CS states of triplet character. This seems to be the case in the data shown in Figure 9. In the case of **PTS3**, the **^{1}PTS3*** formed within about 2 ps revealed ESA peaks at 535, 734, 758, and 898 nm (see Figure 9a). A negative peak at 456 nm representing SE was also observed. Decay/recovery of the ESA/SE peaks resulted in a spectrum with a peak maxima at 637 nm attributable to **^{3}PTS3*** state (see spectrum at 3.97 ps).

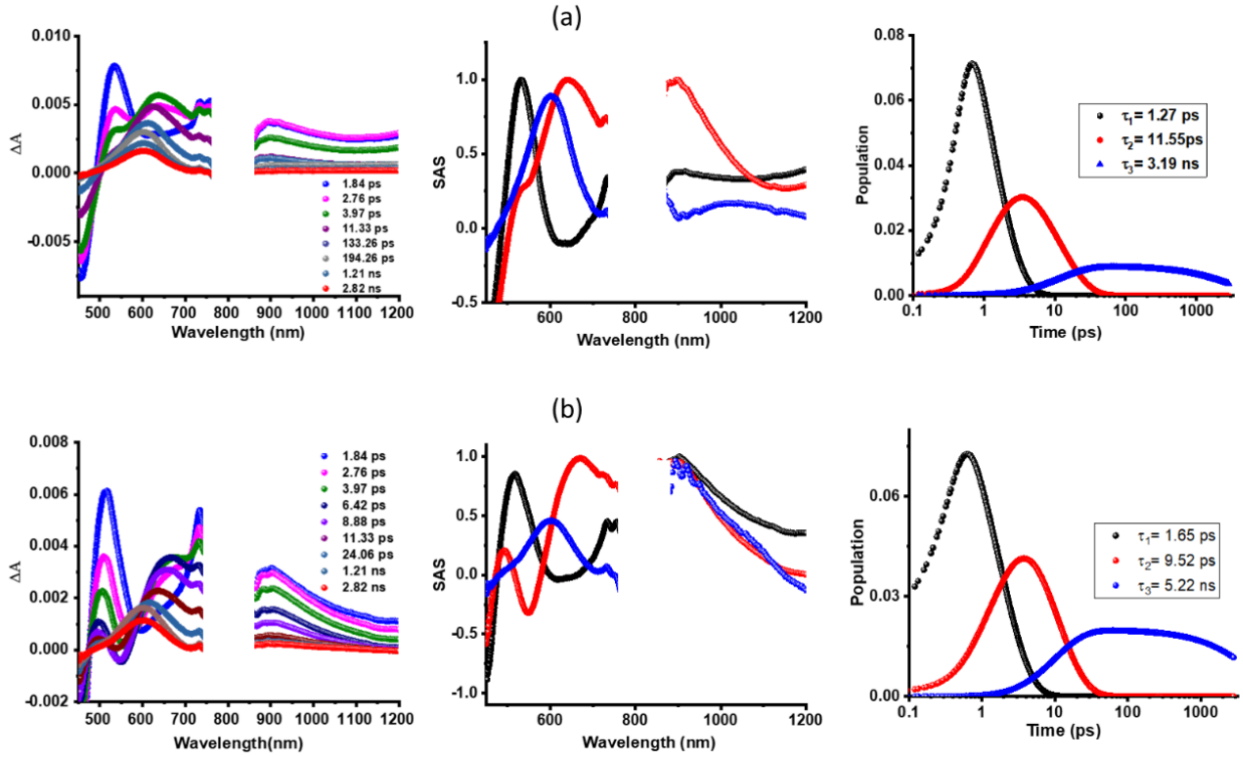

Figure 9. Fs-TA spectra at the indicated delay times of (a) **PTS3** and (b) **PTS 4** at the excitation wavelength of 400 nm. The middle and right-hand panels show, respectively, SAS and population kinetics of different species.

The decay of this peak was associated with a blue shift with a peak maxima at 601 nm. From the earlier discussed spectroelectrochemical results on **PTZ3**, this could be attributed to the charge-separated state (both oxidized and reduced **PTZ3** had positive absorbance in this region as shown in Figure S9b). Glotaran analysis was subsequently performed for a three-component fit representing $S_1 \rightarrow T_1 \rightarrow$ CS processes. The species-associated spectra (SAS) for each species are shown in Figure 9a middle panel while population kinetics are shown right the right-hand panel. The SAS spectra closely resembled that expected for the given species. From population kinetics data, the average lifetimes for T_1 and CS were found to be 11.55 and 3.10 ns. Lifetime for the CS state was generally higher than that reported for other donor-TCBD systems by us and others[30-50] wherein singlet excited state species were involved in promoting CS events. A similar trend representing $S_1 \rightarrow T_1 \rightarrow$ CS processes was observed in the case of **PTS4** (see Figure 9b) wherein the SAS spectra closely resembled that expected for the given species. From population kinetics data, the average lifetimes for T_1 and CS were found to be 9.52 ps and 5.22 ns. We also analyzed

the data by a four-component fit representing S_1 → T_1 → CT → CS processes. However, both CT and CS were very close suggesting these two processes occur almost simultaneously.

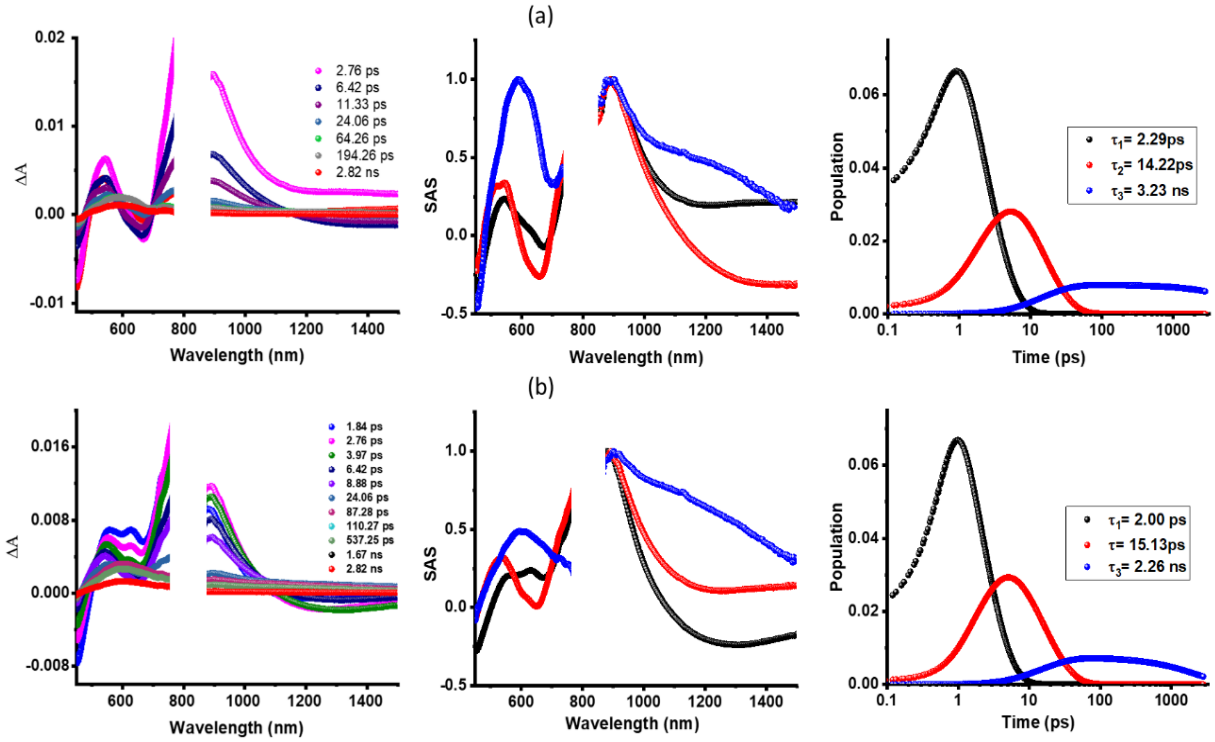

Figure 10. Fs-TA spectra at the indicated delay times of (a) **PTS5** and (b) **PTS6** at the excitation wavelength of 400 nm. The middle and right-hand panels show, respectively, SAS and population kinetics of different species.

Next, fs-TA studies on **PTS5** and **PTS6** carrying a much stronger electron acceptor exTCBD were performed by exciting the samples at 400 nm representing LE excitation. The energy diagram, shown in Figure S8, also predicted the possibility of CT and CS processes originating from the ^{3}PTZ* and ^{3}PTZSO$_2$* thus enhancing the lifetime of the CS products. Figure 10 shows the fs-TA spectra at the indicated delay times, SAS, and population kinetics representing the S_1 → T_1 → CS processes of these two compounds. Spectral appearance in the 800–1000 nm range suggests the strong spectral overlap of different states including the CT state. Thus, the SAS attributed to the T_1 state could have contributions from the CT state also. Our attempts to separate these two events were not fully successful. Importantly, the SAS representing the CS state clearly revealed the expected near-IR peak of **PTZ5**$^{\bullet-}$ in the 1000–1400 nm range confirming its presence.

Lifetimes of the T_1 and CS from population kinetics were found to be 14.22 ps and 3.23 ns for **PTS5** and 15.13 ps and 2.26 ns in the case of **PTS6**. Due to the higher exergonicity of exTCBD systems, faster CS events in **PTS5** and **PTS6** compared to **PTS3** and **PTS4** have been witnessed.

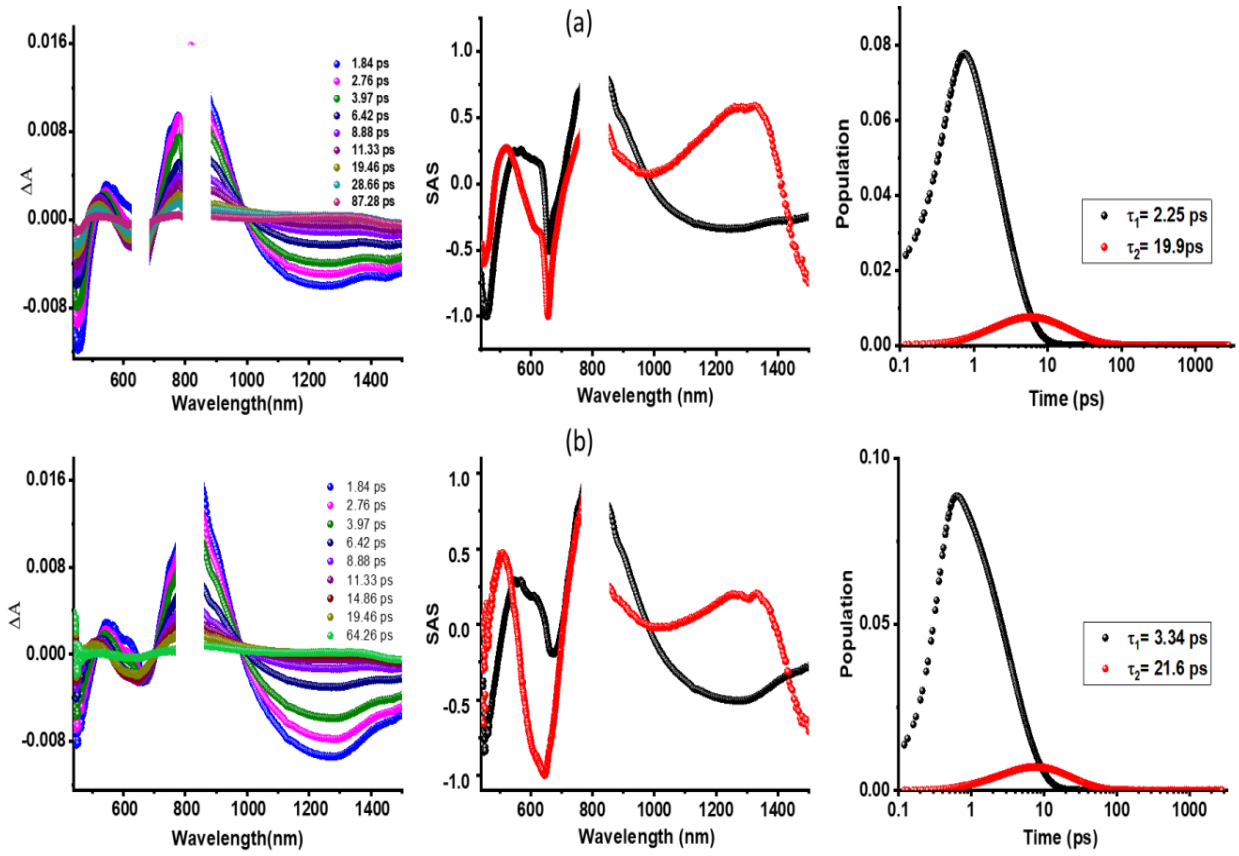

Figure 11. Fs-TA spectra at the indicated delay times of (a) **PTS5** and (b) **PTS6** at the excitation wavelength of 680 nm. The middle and right-hand panels show, respectively, SAS and population kinetics of different photo events.

As discussed earlier, excitation of the **PTS3**–**PTS6** corresponding to their CT state peak position is expected to generate their corresponding ^{1}CT* states, viz., ^{1}[PTZ-(TCBD-PTZSO$_2$)$^{\delta-}$-TCBD-(PTZ)$^{\delta+}$]* in the case of **PTS3**, ^{1}[PTZ-(TCBD)$^{\delta-}$-(PTZSO$_2$-PTZ)$^{\delta+}$]* in the case of **PTS4**, ^{1}[PTZ-(exTCBD-PTZSO$_2$)$^{\delta-}$-(exTCBD-PTZ)$^{\delta+}$]* in the case of **PTS5**, and ^{1}[(PTZ-exTCBD)$^{\delta-}$-(PTZSO$_2$-PTZ)$^{\delta+}$]* in the case of **PTS6**, respectively (derived based on the location of the frontier orbitals in Figure 6). The ^{1}CT* states thus produced could undergo CS, especially in polar benzonitrile utilized here, or relax to the ground state directly. If it undergoes the former process, due to the singlet origin of the charge-separated product, the lifetime of such species

would be much shorter than that discussed earlier for the triplet state originated charge separation. In order to confirm this, fs-TA spectral studies on **PTS3**–**PTS6**, excited at their CT peak maxima, were performed. Figure S10 shows data corresponding to **PTS3** and **PTS4** while Figure 11 shows that of **PTS5** and **PTS6**.

As can be seen from the presented data, all of the photochemical events were completed within about 80 ps for both TCBD or exTCBD bearing push-pull compounds, a good sign that these are ^{1}CT* → CS originated species. The SAS spectra attributed to the CS state matched closely to the earlier discussed results when LE excitation was used, including the near-IR peak in the case of **PTS5** and **PTS6** (see Figure 11). The lifetime of the charge-separated states of singlet character from the analysis of population kinetics was found to be 16.36 ps for **PTS3**, 15.15 ps for **PTS4**, 19.9 ps for **PTS5,** and 21.6 ps for **PTS6**. It may be mentioned here that the spectra associated with the charge-separated state appear slightly different due to different excited state species produced at different wavelengths. These lifetime values are comparable to the lifetime of other Donor-TCBD and Donor-exTCBD systems (Donor = electron-rich photosensitizer), reported earlier,[30-50] all originating from their respective singlet excited states.

Summary

Extension of the lifetime of charge-separated states in strongly interacting push-pull systems by making use of the triplet excited states formed as a function of excitation wavelengths have been successfully demonstrated. To accomplish this task, electron-rich phenothiazine and electron-deficient phenothiazine sulfone were used to form the initial triad. Several interesting properties, including mechanochromism, solvatochromism, and aggregation-induced emission were observed for this triad. The introduction of stronger electron acceptors, TCBD and exTCBD resulted in intramolecular charge transfer both in the ground and excited states. The formation of high-energy triplet states (2.32–2.38 eV) of both phenothiazine and phenothiazine sulfone was established from phosphorescence studies suggesting that they can promote electron transfer resulting in long-lasting, charge-separated states of triplet character irrespective of the nature of electron acceptors, $PZSO_2$ or TCBD/exTCBD due to thermodynamic feasibility of such reactions. This phenomenon was possible to demonstrate using femtosecond transient absorption spectral studies where excitation of the studied push-pull systems corresponding to the locally excited state resulted in the formation of the triplet excited states of the probes by intersystem crossing and due

to their high energy, they were able to promote charge separation. The lifetime of the charge-separated states was much higher than what would be expected from their singlet excited state. Alternatively, excitation of the push-pull systems corresponding to their charge-transfer state also promoted charge separation but due to the singlet character of the products, fast charge recombination was witnessed. The present study brings out the significance of high-energy triplet states and excitation wavelength selection, the two key parameters, in promoting and stabilizing charge separation in highly interacting push-pull systems.

ASSOCIATED CONTENT

Supporting Information

Experimental and synthetic details, ^{1}H and ^{13}C NMR, and MALDI-mass of synthesized compounds. Additional CVs and redox data, spectral data on neutral, oxidized, and reduced compounds, energy diagram, and fs-TA spectral data.

AUTHOR INFORMATION

Corresponding Authors

Rajneesh Misra

Department of Chemistry, Indian Institute of Technology, Indore 453552, India; orcid.org/0000-0003-3225-2125; Email: rajneeshmisra@iiti.ac.in

Francis D'Souza

Department of Chemistry, University of North Texas, 1155 Union Circle, #305070, Denton, TX 76203-5017, USA, orcid.org/0000-0003-3815-8949, E-mail: Francis.DSouza@UNT.edu

Authors

Manju Sheokand

Department of Chemistry, Indian Institute of Technology, Indore 453552, India

Ajyal Z. Alsaleh

Department of Chemistry, University of North Texas, 1155 Union Circle, #305070, Denton, TX 76203-5017, USA

Conflict of Interest

There are no conflicts to declare.

Author Contributions

M.S. and A.Z.A contributed equally to this work.

Acknowledgments

This research was supported by the US-National Science Foundation (2000988 to FD), Council of Scientific and Industrial Research (Project No. CSIR 01(2934)/18/EMR-II), New Delhi, and SERB (Project No. CRG/2018/000032) New Delhi, Govt. of India. We gratefully acknowledge the Sophisticated Instrumentation Centre (SIC), IIT Indore. IY is thankful to CSIR, India for a research fellowship.

References

(1) Deisenhofer, J.; Norris, J. R. *Photosynthetic Reaction Center*; Academic Press: San Diego, CA, 2013; Vol. 2.

(2) Wasielewski, M. R. Self-Assembly Strategies for Integrating Light Harvesting and Charge Separation in Artificial Photosynthetic Systems. *Acc. Chem. Res.* **2009**, *42*, 1910−1921.

(3) Straight, S. D.; Kodis, G.; Terazono, Y.; Hambourger, M.; Moore, T. A.; Moore, A. L.; Gust, D. Energy Conversion in Natural and Artificial Photosynthesis. *Nat. Nanotechnol.* **2008**, *3*, 280−283.

(4) Bottari, G.; de la Torre, G.; Guldi, D. M.; Torres, T. Covalent and Noncovalent Phthalocyanine-Carbon Nanostructure Systems: Synthesis, Photoinduced Electron Transfer, and Application to Molecular Photovoltaics. *Chem. Rev.* **2010**, *110*, 6768−6816.

(5) Guldi, D. M.; Sgobba, V. Carbon Nanostructures for Solar Energy Conversion Schemes. *Chem. Commun.* **2011**, *47*, 606−610.

(6) D'Souza, F.; Ito, O. Photosensitized Electron Transfer Processes of Nanocarbons Applicable to Solar Cells. *Chem. Soc. Rev.* **2012**, *41*, 86−96.

(7) D'Souza, F.; Ito, O. In Multiporphyrin Array: Fundamentals and Applications; Kim, D., Ed.; Pan Stanford Publishing: Singapore, 2012; Chapter 8, pp 389−437.

(8) Imahori, H.; Umeyama, T.; Ito, S. Large π-Aromatic Molecules as Potential Sensitizers for Highly Efficient Dye-Sensitized Solar Cells. *Acc. Chem. Res.* **2009**, *42* (11), 1809–1818.

(9) KC, C. B.; D'Souza, F. Design and Photochemical Study of Supramolecular Donor−Acceptor Systems Assembled via Metal−Ligand Axial Coordination. *Coord. Chem. Rev.* **2016**, *322*, 104−141.

(10) Zhang, J., Xu, W., Sheng, P., Zhao, G. and Zhu, D., Organic donor–acceptor complexes as novel organic semiconductors. *Acc. Chem. Res.,* **2017**, *50*, 1654-1662.

(11) Sommer, M., Huettner, S. and Thelakkat, M., Donor–Acceptor Block Copolymers for Photovoltaic Applications. *J. Mater. Chem.,* **2010**, *20*, 10788–10797.

(12) Deibel, C., Strobel, T. and Dyakonov, V., Role of the Charge Transfer State in Organic Donor–Acceptor Solar Cells. *Adv. Mater.,* **2010,** *22*, 4097–4111.

(13) Balzani, V.; Credi, A.; Venturi, M. Photochemical Conversion of Solar Energy. *ChemSusChem* **2008**, *1*, 26−58.

(14) Armaroli, N.; Balzani, V. The Future of Energy Supply: Challenges and Opportunities. *Angew. Chem., Int. Ed.* **2007**, *46*, 52–66.

(15) Beaujuge, P. M.; Fréchet, J. M. J. Molecular Design and Ordering Effects in π-Functional Materials for Transistor and Solar Cell Applications. *J. Am. Chem. Soc.* **2011**, *133*, 20009–20029.

(16) Hammarström, L. Accumulative Charge Separation for Solar Fuels Production: Coupling Light-Induced Single Electron Transfer to Multielectron Catalysis. *Acc. Chem. Res.* **2015**, *48*, 840–850.

(17) Bottari, G.; Torres, T. *Organic Nanomaterials: Synthesis, Characterization, and Device Applications,* Eds: Torres, T.; Bottari, G. John Wiley & Sons, Inc., Hoboken, NJ, **2013**.

(18) Wu, Y.; Zhu, W. Organic Sensitizers from D–π–A to D–A–π–A: Effect of the Internal Electron-Withdrawing Units on Molecular Absorption, Energy Levels and Photovoltaic Performances. *Chem. Soc. Rev.* **2013**, *42*, 2039–2058.

(19) Misra, R.; Bhattacharyya, S. P. Nonlinear Optical Response of ICT Molecules. *Intramolecular Charge Transfer: Theory and Applications* **2018**.

(20) May, V.; Kühn, O. *Charge and Energy Transfer Dynamics in Molecular Systems*, John Wiley & Sons **2008**.

(21) Fukuzumi, S.; Ohkubo, K.; Suenobu, T. Long-Lived Charge Separation and Applications in Artificial Photosynthesis. *Acc. Chem. Res.* **2014**, *47*, 1455–1464.

(22) Barrejón, M.; Arellano, L. M.; D'Souza, F.; Langa, F. Bidirectional Charge-Transfer Behavior in Carbon-Based Hybrid Nanomaterials. *Nanoscale* **2019**, *11*, 14978–14992.

(23) D. Kim, *Multiporphyrin arrays: Fundamentals and applications*, 2012.

(24) Higashino, T.; Yamada, T.; Yamamoto, M.; Furube, A.; Tkachenko, N. V.; Miura, T.; Kobori, Y.; Jono, R.; Yamashita, K.; Imahori, H. Remarkable Dependence of the Final Charge Separation Efficiency on the Donor-Acceptor Interaction in Photoinduced Electron Transfer. *Angew. Chem., Int. Ed.* **2016**, *55*, 629−633.

(25) Zarrabi, N.; Seetharaman, S.; Chaudhuri, S.; Holzer, N.; Batista, V. S.; van der Est, A.; D'Souza, F.; Poddutoori, P. K. Decelerating Charge Recombination Using Fluorinated Porphyrins in *N,N* -Bis(3,4,5-Trimethoxyphenyl)Aniline—Aluminum(III) Porphyrin—Fullerene Reaction Center Models. *J. Am. Chem. Soc.* **2020**, *142*, 10008–10024.

(26) Canton-Vitoria, R.; Gobeze, H. B.; Blas-Ferrando, V. M.; Ortiz, J.; Jang, Y.; Fernández-Lázaro, F.; Sastre-Santos, Á.; Nakanishi, Y.; Shinohara, H.; D'Souza, F.; Tagmatarchis, N. Excited-State Charge Transfer in Covalently Functionalized MoS2 with a Zinc Phthalocyanine Donor–Acceptor Hybrid. *Angew. Chem., Int. Ed.* **2019**, *58*, 5712–5717.

(27) van Dijk, S. I.; Groen, C. P.; Hartl, F.; Brouwer, A. M.; Verhoeven, J. W. Long-Lived Triplet State Charge Separation in Novel Piperidine-Bridged Donor−Acceptor Systems. *J. Am. Chem. Soc*. **1996**, *118*, 8425−8432.

(28) Obondi, C. O.; Lim, G. N.; Churchill, B.; Poddutoori, P. K.; van der Est, A.; D'Souza, F. Modulating the Generation of Long-Lived Charge Separated States Exclusively from the Triplet Excited States in Palladium Porphyrin−Fullerene Conjugates. *Nanoscale* **2016**, *8*, 8333−8344.

(29) Kivala, M.; Boudon, C.; Gisselbrecht, J.-P.; Seiler, P.; Gross, M.; Diederich, F. Charge-Transfer Chromophores by Cycloaddition–Retro-Electrocyclization: Multivalent Systems and Cascade Reactions. *Angew. Chem., Int. Ed.* **2007**, *46*, 6357–6360.

(30) Michinobu, T.; Diederich, F. The [2+2] Cycloaddition-Retroelectrocyclization (CA-RE) Click Reaction: Facile Access to Molecular and Polymeric Push-Pull Chromophores. *Angew. Chem., Int. Ed.* **2018**, *57*, 3552–3577.

(31) Sekita, M.; Ballesteros, B.; Diederich, F.; Guldi, D. M.; Bottari, G.; Torres, T. Intense Ground-State Charge-Transfer Interactions in Low-Bandgap, Panchromatic Phthalocyanine-Tetracyanobuta-1,3-diene Conjugates. *Angew. Chem., Int. Ed.* **2016**, *55*, 5560−5564.

(32) Winterfeld, K. A.; Lavarda, G.; Guilleme, J.; Sekita, M.; Guldi, D. M.; Torres, T.; Bottari, G. Subphthalocyanines Axially Substituted with a Tetracyanobuta-1,3-diene−Aniline Moiety: Synthesis, Structure, and Physicochemical Properties. *J. Am. Chem. Soc*. **2017**, *139*, 5520−5529.

(33) Leliege, A., Blanchard, P., Rousseau, T. and Roncali, J., Triphenylamine/tetracyanobutadiene-based DAD π-conjugated systems as molecular donors for organic solar cells. *J. Org. Lett.* **2011**, *13*, 3098−3101.

(34) Shoji, T.; Ito, S. Azulene-Based Donor–Acceptor Systems: Synthesis, Optical, and Electrochemical Properties. *Chem. Eur. J.* **2017**, *23*, 16696–16709.

(35) Simón Marqués, P.; Castán, J. M. A.; Raul, B. A. L.; Londi, G.; Ramirez, I.; Pshenichnikov, M. S.; Beljonne, D.; Walzer, K.; Blais, M.; Allain, M.; Cabanetos, C.; Blanchard, P. Triphenylamine/Tetracyanobutadiene-Based π-Conjugated Push–Pull Molecules End-Capped with Arene Platforms: Synthesis, Photophysics, and Photovoltaic Response. *Chem. Eur. J.* **2020**, *26*, 16422–16433.

(36) Winterfeld, K. A.; Lavarda, G.; Guilleme, J.; Guldi, D. M.; Torres, T.; Bottari, G. Subphthalocyanine–Tetracyanobuta-1,3-Diene–Aniline Conjugates: Stereoisomerism and Photophysical Properties. *Chem. Sci.* **2019**, *10*, 10997–11005.

(37) Bui, A. T.; Philippe, C.; Beau, M.; Richy, N.; Cordier, M.; Roisnel, T.; Lemiègre, L.; Mongin, O.; Paul, F.; Trolez, Y. Synthesis, Characterization and Unusual near-Infrared Luminescence of 1,1,4,4-Tetracyanobutadiene Derivatives. *Chem. Commun.* **2020**, *56*, 3571–3574.

(38) Gotfredsen, H.; Neumann, T.; Storm, F. E.; Muñoz, A. V.; Jevric, M.; Hammerich, O.; Mikkelsen, K. V.; Freitag, M.; Boschloo, G.; Nielsen, M. B. Donor−Acceptor-Functionalized Subphthalocyanines for Dye-Sensitized Solar Cells. *ChemPhotoChem* **2018**, *2*, 976–985.

(39) Gautam, P.; Misra, R.; Thomas, M. B.; D'Souza, F. Ultrafast Charge-Separation in Triphenylamine-BODIPY-Derived Triads Carrying Centrally Positioned, Highly Electron-Deficient, Dicyanoquinodimethane or Tetracyanobutadiene Electron-Acceptors. *Chem. Eur. J.* **2017**, *23*, 9192−9200.

(40) Sharma, R.; Thomas, M. B.; Misra, R.; D'Souza, F. Strong Ground- and Excited-State Charge Transfer in C3-Symmetric Truxene-Derived Phenothiazine-Tetracyanobutadine and Expanded Conjugates. *Angew. Chem. Int. Ed.* **2019**, *131*, 4394−4399.

(41) Rout, Y.; Jang, Y.; Gobeze, H. B.; Misra, R.; D'Souza, F. Conversion of Large-Bandgap Triphenylamine–Benzothiadiazole to Low-Bandgap, Wide-Band Capturing Donor–Acceptor Systems by Tetracyanobutadiene and/or Dicyanoquinodimethane Insertion for Ultrafast Charge Separation. *J. Phys. Chem. C* **2019**, *123*, 23382–23389.

(42) Poddar, M.; Jang, Y.; Misra, R.; D'Souza, F. Excited-State Electron Transfer in 1,1,4,4-Tetracyanobuta-1,3-Diene (TCBD)- and Cyclohexa-2,5-Diene-1,4-Diylidene-Expanded TCBD-Substituted BODIPY-Phenothiazine Donor–Acceptor Conjugates. *Chem. Eur. J.* **2020**, *26*, 6869–6878.

(43) Pinjari, D.; Alsaleh, A. Z.; Patil, Y.; Misra, R.; D'Souza, F. Interfacing High-Energy Charge-Transfer States to a Near-IR Sensitizer for Efficient Electron Transfer upon Near-IR Irradiation. *Angew. Chem., Int. Ed.* **2020**, *59*, 23697–23705.

(44) Yadav, I. S.; Alsaleh, A. Z.; Misra, R.; D'Souza, F. Charge Stabilization via Electron Exchange: Excited Charge Separation in Symmetric, Central Triphenylamine Derived, Dimethylaminophenyl–Tetracyanobutadiene Donor–Acceptor Conjugates. *Chem. Sci.* **2021**, *12* (3), 1109–1120.

(45) Jang, Y.; Rout, Y.; Misra, R.; D'Souza, F. Symmetric and Asymmetric Push–Pull Conjugates: Significance of Pull Group Strength on Charge Transfer and Separation. *J. Phys. Chem. B* **2021**, *125*, 4067–4075.

(46) Khan, F.; Jang, Y.; Patil, Y.; Misra, R.; D'Souza, F. Photoinduced Charge Separation Prompted Intervalence Charge Transfer in a Bis(Thienyl)Diketopyrrolopyrrole Bridged Donor-TCBD Push-Pull System. *Angew. Chem., Int. Ed.* **2021**, *60*, 20518–20527.

(47) Shinde, J.; Thomas, M. B.; Poddar, M.; Misra, R.; D'Souza, F. Does Location of BF2-Chelated Dipyrromethene (BODIPY) Ring Functionalization Affect Spectral and Electron Transfer Properties? Studies on α-, β-, and Meso-Functionalized BODIPY-Derived Donor–Acceptor Dyads and Triads. *J. Phys. Chem. C* **2021**, *125*, 23911–23921.

(48) Sekaran, B.; Dawson, A.; Jang, Y.; MohanSingh, K. V.; Misra, R.; D'Souza, F. Charge-Transfer in Panchromatic Porphyrin-Tetracyanobuta-1,3-Diene-Donor Conjugates: Switching the Role of Porphyrin in the Charge Separation Process. *Chem. Eur. J.* **2021**, *27*, 14335–14344.

(49) Yadav, I. S.; Jang, Y.; Rout, Y.; Thomas, M. B.; Misra, R.; D'Souza, F. Near-IR Intramolecular Charge Transfer in Strongly Interacting Diphenothiazene-TCBD and Diphenothiazene-DCNQ Push-Pull Triads. *Chem. Eur. J.* **2022**, *28*, e202200348.

(50) Rout, Y.; Motanari, C.; Pasciucco, E.; Misra, R.; Carlotti, B. Tuning the Fluorescence and the Intramolecular Charge Transfer of Phenothiazine Dipolar and Quadrupolar Derivatives by Oxygen Functionalization, *J. Am. Chem. Soc*. **2021**, *143*, 9933-9943.

(51) Rout, Y.; Gautam, P.; Misra, R. Unsymmetrical and Symmetrical Push–Pull Phenothiazines. *J. Org. Chem.* **2017**, *82*, 6840–6845.

(52) Ekbote, A., Mobin, S.M. and Misra, R., Stimuli-responsive phenothiazine-based donor–acceptor isomers: AIE, mechanochromism and polymorphism. *J. Mater. Chem. C*, **2020,** *8*, 3589 −3602.

(53) Tu, L.; Xie, Y.; Li, Z. Advances in Pure Organic Mechanoluminescence Materials, *J. Phys. Chem. Lett*. **2022**, *13*, 5605-5617.

(54) Frisch, M. J.; Trucks, G. W.; Schlegel, H. B.; Scuseria, G. E.; Robb, M. A.; Cheeseman, J. R.; Scalmani, G.; Barone, V.; Mennucci, B.; Petersson, G. A.; Nakatsuji, H.; Caricato, M.; Li, X.; Hratchian, H. P.; Izmaylov, A. F.; Bloino, J.; Zheng, G.; Sonnenberg, J. L.; Hada, M.; Ehara, M.; Toyota, K.; Fukuda, R.; Hasegawa, J.; Ishida, M.; Nakajima, T.; Honda, Y.; Kitao, O.; Nakai, H.; Vreven, T.; Montgomery, J. A., Jr.; Peralta, J. E.; Ogliaro, F.; Bearpark, M.; Heyd, J. J.; Brothers, E.; Kudin, K. N.; Staroverov, V. N.; Kobayashi, R.; Normand, J.; Raghavachari, K.; Rendell, A.; Burant, J. C.; Iyengar, S. S.; Tomasi, J.; Cossi, M.; Rega, N.; Millam, N. J.; Klene, M.; Knox, J. E.; Cross, J. B.; Bakken, V.; Adamo, C., Jaramillo, J.; Gomperts, R.; Stratmann, R. E.; Yazyev, O.; Austin, A. J.; Cammi, R.; Pomelli, C.; Ochterski, J. W.; Martin, R. L.; Morokuma, K.; Zakrzewski, V. G.; Voth, G. A.; Salvador, P.; Dannenberg, J. J.; Dapprich, S.; Daniels, A. D.; Farkas, O.; Foresman, J. B.; Ortiz, J. V.; Cioslowski, J.; Fox, D. J. Gaussian 09, Revision A.02; Gaussian, Inc., Wallingford, CT, 2009.

(55) Rehm, D.; Weller, A. Kinetics of Fluorescence Quenching by Electron and H-Atom Transfer. *Isr. J. Chem.* **1970**, *8*, 259–271.

(56) Snellenburg, J. J.; Laptenok, S.; Seger, R.; Mullen; K. M.; van Stokkum, I. H. Glotaran: A Java-based graphical user interface for the R package TIMP. *J. Stat. Softw.* **2012**, *49*, 1–22.

(57) Ekbote, A., Han, S.H., Jadhav, T., Mobin, S.M., Lee, J.Y. and Misra, R., Stimuli responsive AIE active positional isomers of phenanthroimidazole as non-doped emitters in OLEDs. *J. Mater. Chem. C*, **2018**, *6*(8), 2077–2087.

Table of contents